IOP Conf. Series: Earth and Environmental Science **1411** (2024) 012068 doi:10.1088/1755-1315/1411/1/012068

On the Generation of Large-Scale Vortical Flow Structures in Pipe Multifurcations

Bernhard Semlitsch
TU Wien, Getreidemarkt 9/BA, Vienna 1060, Austria
E-mail: bernhard.semlitsch@tuwien.ac.at

Abstract. In many hydraulic power plants, the water supplied through the penstock needs to be distributed to multiple turbines. The application of pipe multifurcations is motivated by economic and efficiency reasoning. However, flow instabilities and large-scale vortical flow structures can occur for some operating conditions, causing high-amplitude pressure and mass flow rate fluctuations. To enhance the understanding of the flow instability inception, we investigate the unsteady flow in a pipe multifurcation with six branches for different operating conditions. The unsteady flow is simulated employing the large eddy simulation approach, where the numerical mesh is constructed such that $y^+ < 1$ and a recycling-type boundary condition is utilised to provide the turbulent inflow conditions. While the general flow pattern are described by the time-averaged results, the work focuses on analysing the unsteady physical phenomena occurring in the pipe multifurcation. At part-load operation, the results clearly show the formation of large-scale vortical flow structures stretching into the active branches. The vortices are observed to move around and eventually burst. When one vortex breaks down, the other large-scale vortices reaching into the other active branches are likely to burst and the flow pattern changes. Such events come with decreased turbulence intensity propagating through the branch line, flow separation at the branch line junction, and mass flow rate fluctuations. After a short time, large-scale vortices were established again.

Keywords: penstock flows, multifurcations, unsteady flow, coherent flow structures, numerical flow simulation

1. Introduction

Grid flexibility is crucial in modern electric power generation [1]. Fast reaction times over a wide range of operating conditions are desired from the electric power system to satisfy the demand. Only combining several machines allows the coverage of mass flow rate ranges to provide flexibility at high efficiencies. Pipe junctions are used to distribute the proportional energy carried by the water masses from and to the machines. Also, Pelton and Turgo turbines with multiple nozzles exhibiting excellent performance over the operating range require well-designed manifolds. Pipe multifurcations provide economic advantages due to their compactness over sequences of Y-junctions [2] but generate higher hydraulic losses than single systems [9]. Nonetheless, large flow distortions and pressure fluctuations are often observed in trifurcations [3]. Thus, risk assessment of developing flow instabilities is imperative before installing pipe multifurcations [4].

Multiple researchers investigated the formation of flow instabilities in trifurcations using numerical simulations. Ruprecht et al. [5] analysed the vortical flow structure generation in

a trifurcation with a spherical shape and highlighted the need for scale-resolving simulations. Unsteady Reynolds-Averaged Navier-Stokes (RANS) simulations were incapable of predicting the vortex structure correctly. In contrast, the very large eddy simulation approach captured the alternating occurrence of the vortex in accordance with the observations in the power plant. Kirschner et al. [6] investigated the occurrence of vortical flow structures in a trifurcation numerically and experimentally. The observed flow pattern was highly dependent on the operating condition. The pressure fluctuations could be mitigated by reducing the dead water space at the junction. Hyun et al. [2] reports 18% power output fluctuations of the turbine caused by the generated flow structures in a trifurcation. The oscillating nature of the vortical flow jumping from the upper to the lower cavity could be simulated using an unsteady Reynolds-Averaged Navier-Stokes simulation approach, where the $k-\varepsilon$ turbulence closure model was used. Guo et al. [7] employed the large eddy simulations to investigate the flow field pulsations of over 15 m^3/s or 10 MW in a spherical trifurcation. Morabito et al. [8] applied the realizable $k-\varepsilon$ turbulence closure model to simulate the flow structure generation in a pipe trifurcation under many operating conditions. The flow structures and their turbulence levels were shown to significantly impact the downstream turbine's performance. Decaix et al. [4] reported that the prediction of the flow stability behaviour in the trifurcation varied for different turbulence models. Aguirre et al. [9] investigated the loss coefficients and mass flow rate variations in a pipe trifurcation. The computational results revealed a strong dependency on the numerical mesh and the turbulence modelling.

Predicting the flow stability in multifurcations is challenging. Nonetheless, consent prevails for the mitigation method, limiting the dead water regions to a minimum. However, not all multifurcations allow this strategy to be applied. We investigate a manifold geometry with six branch lines distributed around the circumference under several operating conditions, where dead water regions cannot be avoided because of the spatial requirements of the junctions. The large eddy simulation approach is applied to accurately capture the formation of the vortical flow structure. A recycling-type inflow boundary condition is used to obtain realistic and representative flow conditions in the junction element. The large-scale flow structures are visualised, and their dynamic motion is analysed.

2. Methodology and Setup

The investigated manifold geometry with six equidistributed branch lines is shown in figure 1, which represents a typical flow distributor for Pelton or Turgo turbines. The inlet pipe has a diameter of 0.26 m and is ten inlet pipe diameters long. The junction element starts as a conical diffuser, has six perpendicular tightly and equally spaced branch arms with an initial conical convergent section, and is axially closed by a hemisphere. All branch lines have the same diameter of 0.1354 m. The flowing medium is water with a density of $\varrho = 1000$ kg/m^3, and a kinematic viscosity of $\nu = 1 \cdot 10^{-6}$ m^2/s. The static pressure is set at the open outlets as standard atmospheric conditions. The mass flow rates are set proportionally at the inlet to represent different operating conditions corresponding to one, two, three, four, and six active branches. The mass flow rate is 182.4 kg/s for six active branches, corresponding to a Reynolds number of $1,000,000$.

Solutions of the three-dimensional Navier-Stokes equations are computed using OpenFOAM v2312 to simulate the vortical flow structure generation in the incompressible water flow. The set of equations can be written as,

$$\nabla \mathbf{u} = 0 \tag{1}$$

$$\frac{\partial \mathbf{u}}{\partial t} + (\mathbf{u} \cdot \nabla)\mathbf{u} = -\frac{1}{\rho}\nabla p + \nu \nabla^2 \mathbf{u} \ , \tag{2}$$

where $\mathbf{u}$ is the three-dimensional flow velocity, ϱ is the fluid density, p is the static pressure, and ν is the kinematic viscosity. The viscous forces can be expected to be tiny due to the typically

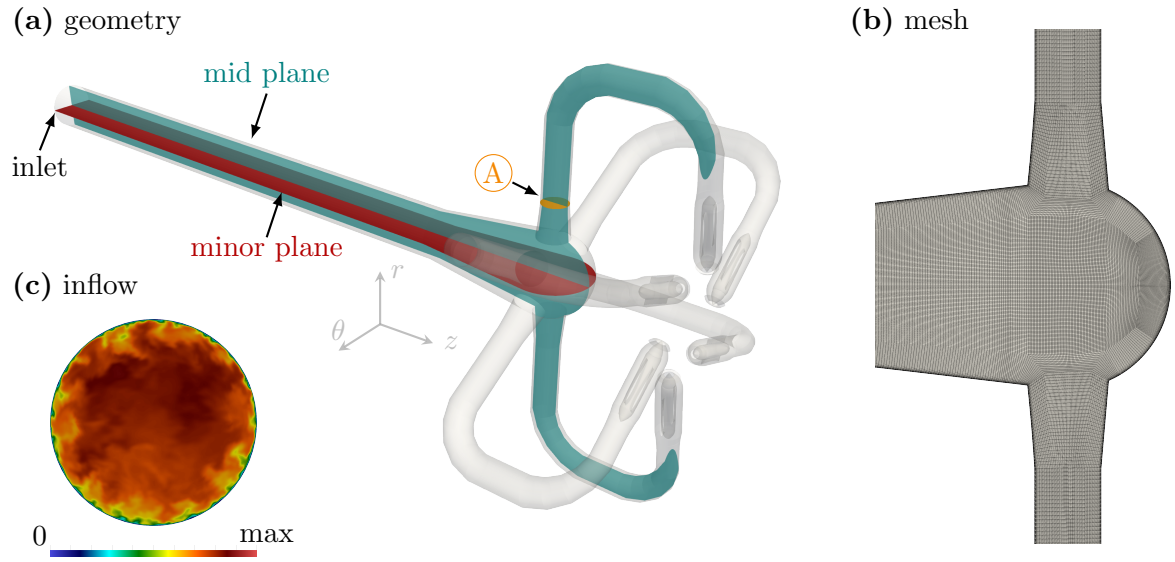

Figure 1. The investigated pipe geometry with multifurcations is shown in subfigure (a). A detail of the numerical mesh is plotted in subfigure (b) in the mid-plane view. The subfigure (c) shows a typical turbulent velocity distribution imposed at the inlet.

high Reynolds number in hydraulic pipes. Resolving all scales on the numerical discretisation demands an excess of computational resources and, therefore, only the large coherent flow structures are resolved. In contrast, the flow scales smaller than the mesh resolution are modelled using the Wall-Adapting Local Eddy-viscosity (WALE) sub-grid-scale model with standard coefficients.

The *piso* algorithm is utilised to solve the pressure-velocity coupling, where 3 corrector iterations with one non-orthogonal correction are performed at each time step. The backward scheme is used for time discretisation with a constant time step of $1 \cdot 10^{-5}$ s satisfying that the Courant number is smaller 0.5 at all times. All gradients are computed using a cell value-limited least squares scheme. A linear Gaussian scheme is used to discretise all Laplace operations. The SuperBee scheme is employed for the divergence operators due to its low dissipative error. Linear interpolation is performed to transfer information between the cell points and the face midpoints.

No slip wall boundary conditions are applied to all solid walls. The static pressure is set at the open branch outlets. A recycling-type boundary condition is employed at the inlet. Therefore, the unsteady velocity profile is extracted from eight inlet pipe diameters downstream of the inlet, rescaled to match the target mass flow rate, and imposed at the inlet. A typical turbulent velocity distribution imposed at the inlet is illustrated in figure 1 (c).

The computational domain is discretised by a fully block-structured mesh consisting of over 120 million hexahedral cells, which is shown in figure 1 (b). Refinements have been applied towards all solid walls to achieve $y^+ < 1$ in the entire domain. A coarsening sponge layer (replacing the nozzles shown in figure 1) was implemented towards all outlets to enhance the simulation stability. That the mesh resolution, in combination with the selected numerical schemes, is suitable for large eddy simulations has been verified by computing the Pope index [10] and the LES_IQ [11, 12], which are shown in figure 2.

3. Results

Figure 3 shows the time-averaged velocity magnitude contours for different operating conditions in the mid-plane, minor-plane, and (A)-plane view. The penstock inflow velocities are

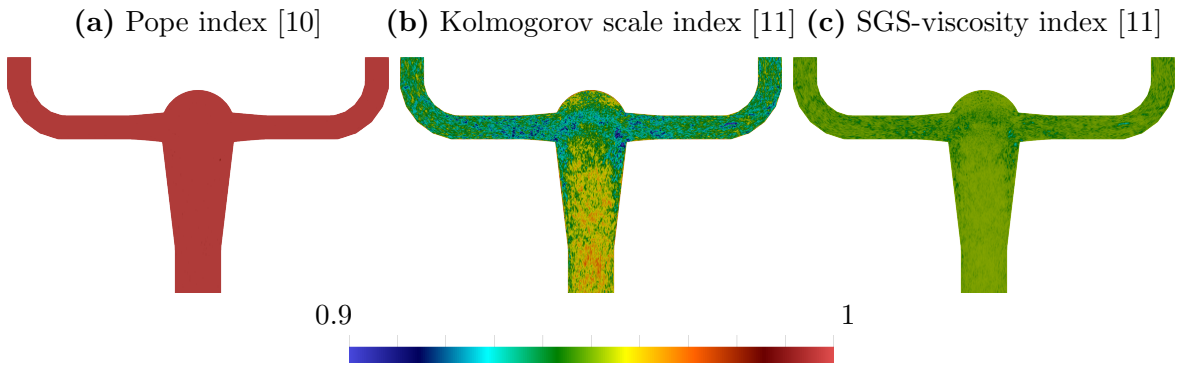

Figure 2. The large-eddy simulation quality indices are show in the mid-plane view for the case with four active branch lines. The suggested values by Celik et al. [11, 12] have been adopted for required parameters.

proportional to the number of active branch lines. With only one active branch line, the inflow velocities into the diffuser are so low that no flow separation at the diffuser walls can be observed. The flow enters the branch line unperturbed but has a higher axial flow momentum, causing flow separation at the branch line edge facing the inlet. Thereby, counter-rotating Dean-vortex pairs are generated, which are visible in the (A)-plane view and the flow is pushed against the outer branch line wall. At the subsequent 90° pipe bend, other counter-rotating Dean-vortex pairs are induced, which rotate in the opposite direction than the pair originating from the pipe multifurcation. The strength of these second Dean-vortex pairs is suppressed by the first Dean-vortex pairs, which forces the flow against the outer pipe wall and delays, thereby, the flow separation and formation of the second counter-rotating Dean-vortex pairs.

With all six branch lines in operation, the axial flow momentum is significantly higher in the penstock. Therefore, the central flow reaches the cap of the pipe multifurcation and is redirected into the branch lines. Because the axial flow exhibits a higher momentum than the redirected flow, flow separation is triggered at the branch line edge facing the inlet. Figure 3 shows that the flow topology in the branch line is similar to that described for the single branch line operation.

The flow characteristics evolve distinctively when two but not all branch lines are active. A large-scale vortex is visible in front of the inactive branch lines, which can be clearly seen in the minor-plane view shown in figure 3. Notably, the large-scale vortex cores are located between the pipe multifurcation cap and the branch line axes. The flow momentum in the axial downstream direction is higher (exerting the force on the large-scale vortical flow structure) because only a part of the penstock flow is redirected at the pipe multifurcation cap while the other part enters the branch line directly. Also, the flow pattern in the branch lines is affected by the large-scale vortical flow structures. Flow separation and counter-rotating Dean-vortex pairs are less clearly visible. The large-scale vortical flow structures extend into the active branch lines and interact with the flow characteristics described for one and six active branch lines. The relatively weak vortex, being generated when two branch lines are active, joins one of the Dean-vortices, causing less flow symmetry in the branch lines. Three large-scale vortical flow structures are provoked when three branch lines are active, which form a counter-rotating vortex pair entering the branch line. This counter-rotating vortex pair has sufficient strength to change the flow pattern at the branch line junction. Two main large-scale vortical flow structures are initiated when four branch lines are active, where one end of the large-scale vortical flow structures stretches into each active branch line. Because of their strength, the flow pattern in the branch line is entirely dominated by these large-scale vortical flow structures.

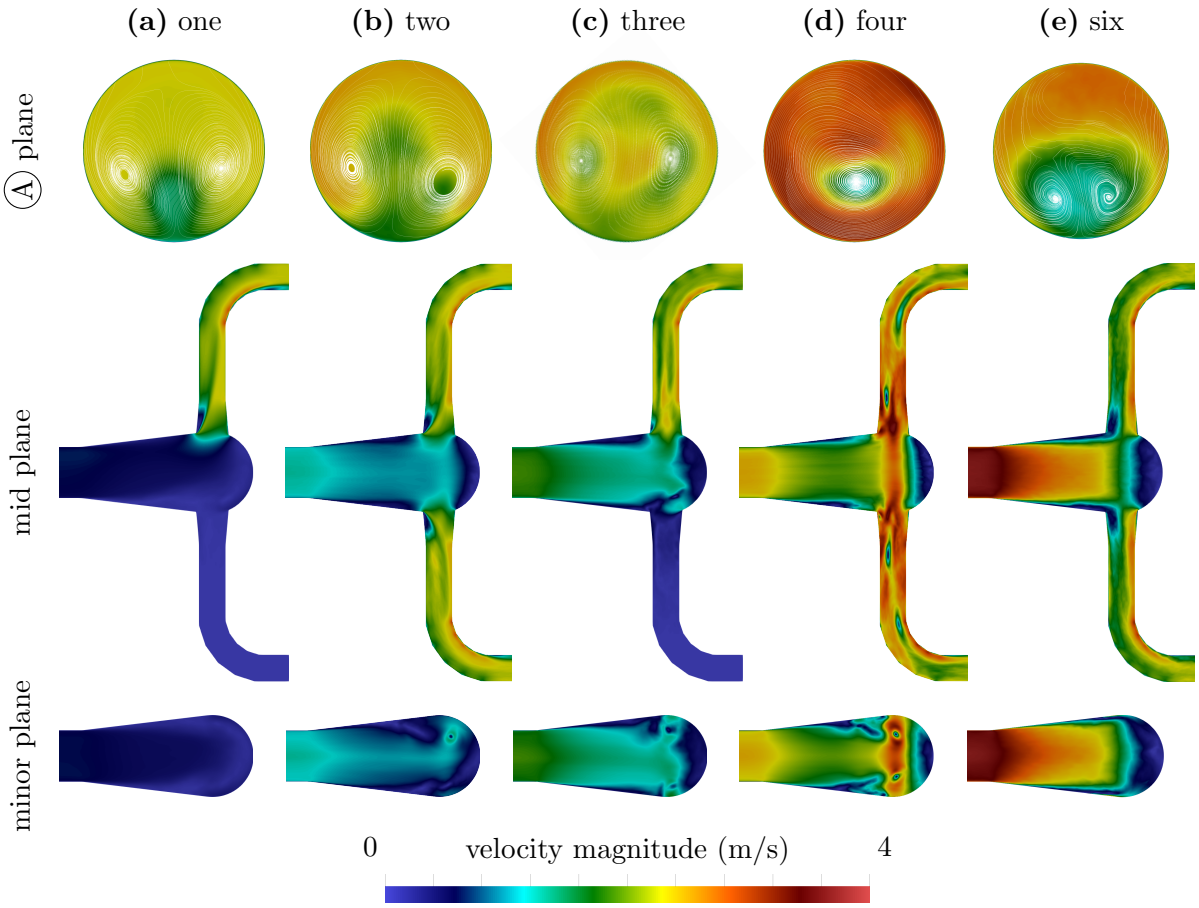

Figure 3. The time-averaged velocity magnitude contours are shown in the mid, the minor, and the Ⓐ-plane view for different numbers of branch lines in operation. The plane view locations are indicated in figure. 1.

3.1. Large-scale vortical flow structures

The general flow field, described in Section 3, indicated that large-scale flow instabilities are present with two to four active branch lines. These flow structures are illustrated in figure 4 at representative time steps. Large-scale vortical flow structures form for each active branch line, where the other ends connect to the neighbouring active branch lines. These flow structures affect the flow separation at the branch line junction and can entirely suppress its occurrence. Figure 4 shows that the large-scale vortical flow structures are weaker when fewer branch lines are active. Thus, the impact on the branch line flow is less, as illustrated in the Ⓐ-plane depicted in figure 3. When four branch lines are active, the large-scale vortical flow structures dominate the flow pattern in the branch line. The ends of the large-scale vortical flow structures cause amplified turbulence in the active branch lines, resulting in a large pressure drop. Therefore, the pressure is significantly higher in the penstock when two to four branch lines are active compared to the operating conditions with one or all active branch lines. Counter-rotating vortex pairs from in each active branch line when three branch lines are active, while mostly one dominant large-scale vortical flow structure is present in each active branch line when two or four branch lines are active.

The large-scale vortical flow structures are energised by the main flow in the penstock as

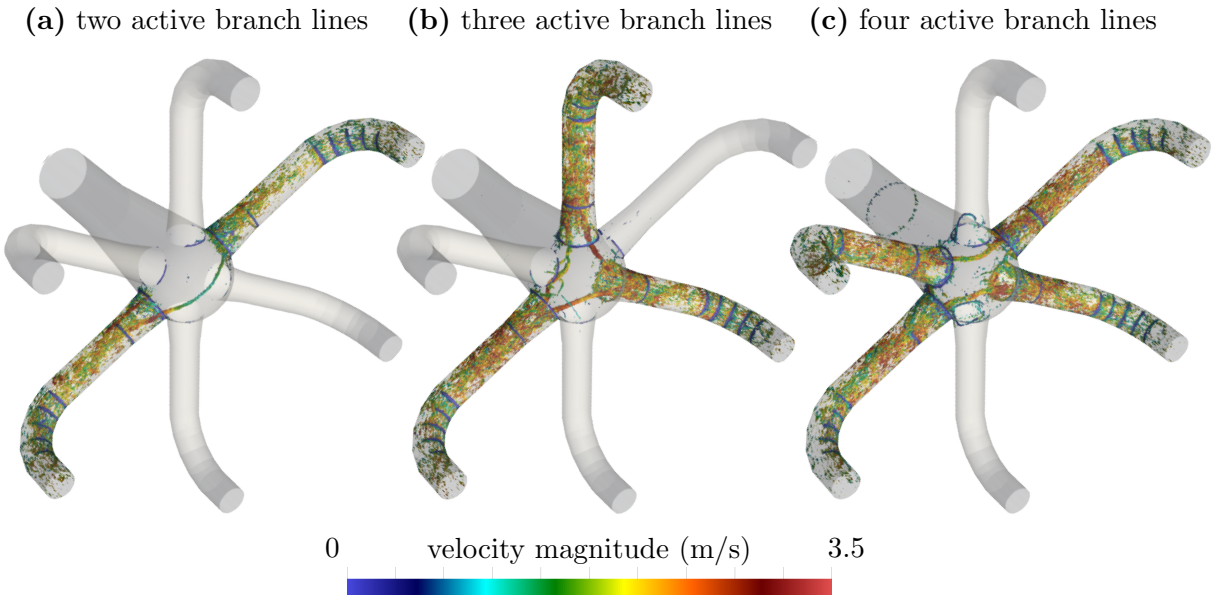

Figure 4. The vortical flow structures are shown by iso-surfaces of the Q-criterium coloured by the velocity magnitude for different numbers of branch lines in operation. The same Q-criterium value has been chosen for all branch line operation cases.

illustrated in figure 5.[1] The axial flow needs to turn 90° to enter the active branch lines, and therefore, axial forces are required. Because of the diffuser divergence and the branch lines being distributed around the outer circumference, the axial flow momentum is higher in the centre

[1] The counter-rotating vortex pairs appear first in the entrance region into the branch line junctions due to the flow acceleration amplifying vorticity.

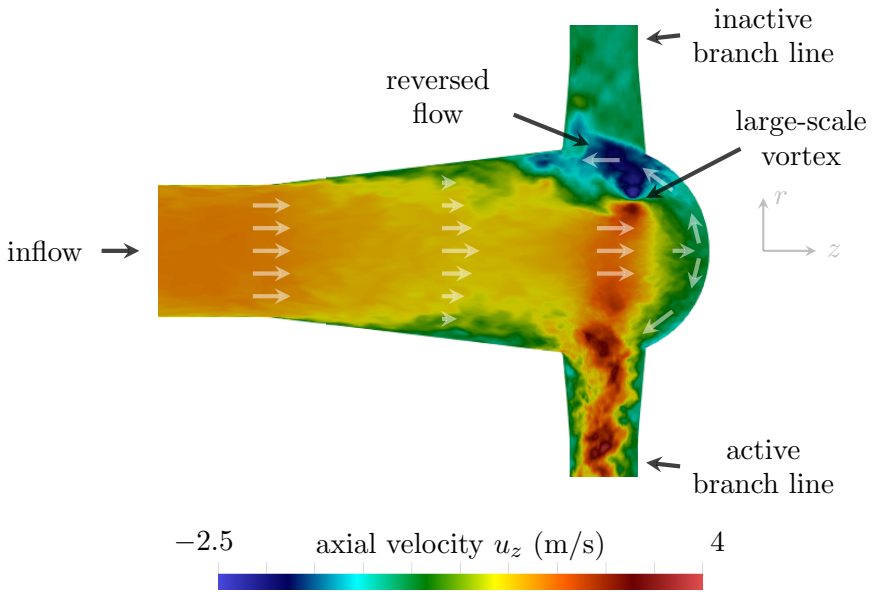

Figure 5. The amplification of the large-scale vortical flow structures by the mean flow is illustrated for the operating condition with three active nozzles in the mid-plane view.

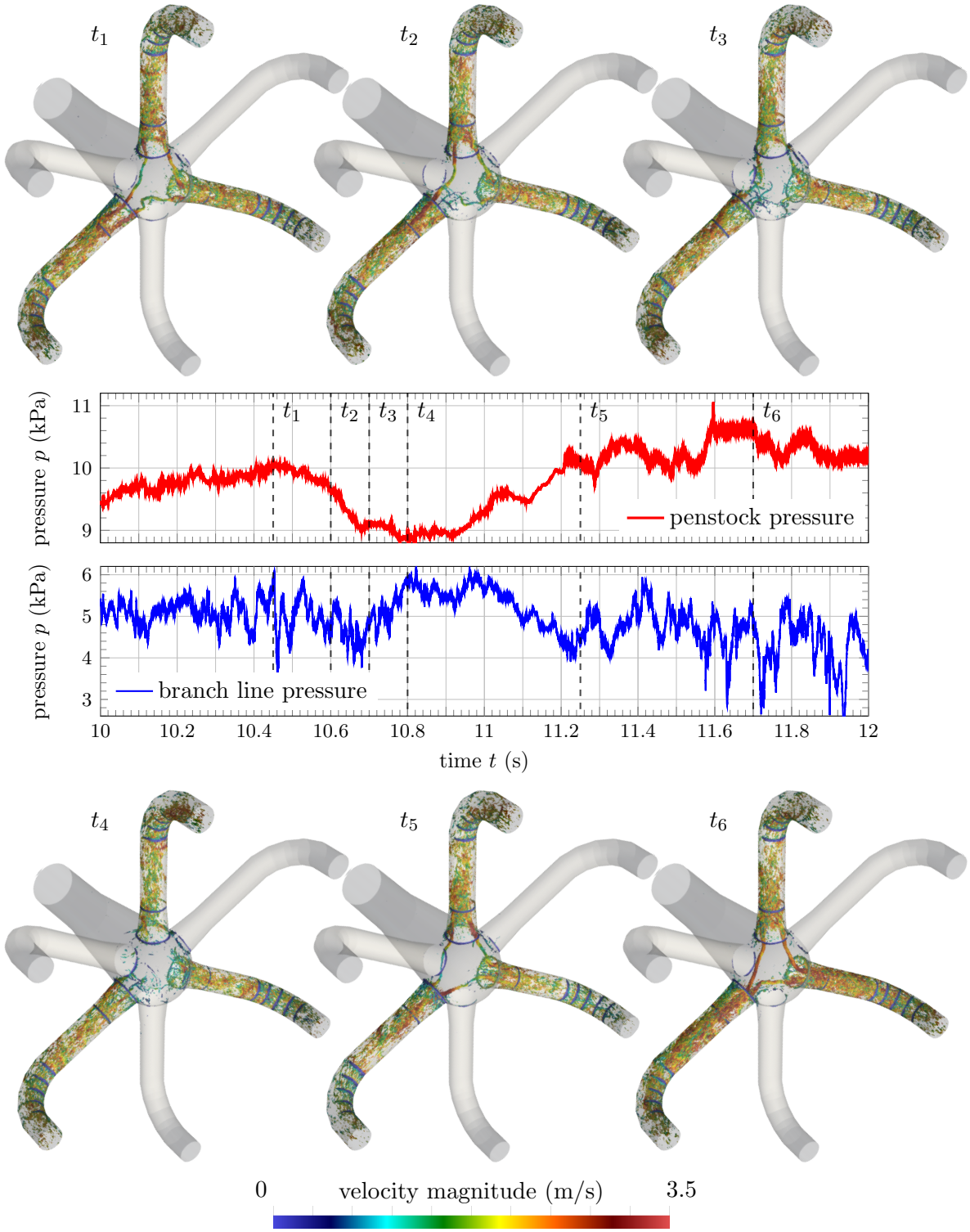

Figure 6. The evolution of the large-scale vortical flow structures is visualised by iso-surfaces of the Q-criterion coloured by the velocity magnitude at selected time steps. The history of pressure in the penstock and the branch line quantifies the impact of the formation and disruption of large-scale vortical flow structures.

of the pipe multifurcation. Therefore, the axial flow is redirected at the hemispherical cap of the pipe multifurcation towards the outer periphery. The reversed flow joins the main flow into the active branch lines. In between active branch lines, the reversing flow and the mean flow generate a shear flow feeding the large-scale vortices. Figure 4 shows that the size and strength of the vortical flow structures depend on both the space given to the reversing flow and the axial velocity magnitude in the pipe multifurcation penstock. Both influence factors are directly but oppositely related to the number of active branch lines.

Figure 6 illustrates the extensive movement of the large-scale vortical flow structures in the pipe multifurcation, which eventually burst and are reestablished shortly thereafter. The large-scale vortical flow structures unravel as small, turbulent flow structures in the active branch lines. This causes an increased pressure drop over the branch line junction. Figure 6 shows that the stronger the large-scale vortical flow structures become, the higher the pressure in the penstock. The pressure in the pipe multifurcation decreases suddenly when the large-scale vortical flow structures burst (at the time 10.5 s). With the bursting event, the flow fluctuations in the branch line reach extreme amplitudes. Once the residuals of the large-scale vortical flow structures have been drained, the flow in the active branch lines exhibits less turbulent flow structures, and flow separation occurs at the branch line junctions facing the penstock inlet. Thereafter, the large-scale vortical flow structures appear again, and the pressure in the penstock rises.

Several phenomena causing the burst of large-scale vortices have been observed. The cores of the large-scale vortices are located mainly further downstream in the axial direction than the branch line centres. Therefore, the vortical flow structure drains fluid from the inactive branch line, where the static pressure decreases. Due to the lower static pressure, the large-scale vortices are dragged towards the inactive branch line. There, the eventual interaction with the solid surfaces disrupts the large-scale vortical flow structures. Another flow phenomenon leading to the burst of large-scale vortices is their extensive motion and deformation. The displacement can be severe enough that a large-scale vortex bursts. When one large-scale vortex bursts, the other large-scale vortices are affected by the triggered flow unsteadiness and can burst as well.

4. Discussion

The investigated geometry has a particular shape. Nonetheless, general conclusions can be drawn guiding the pipe multifurcation design. The flow momentum needs to be turned by the manifold into the branch lines for all operating conditions. The present work demonstrated that avoiding the driving source of the large-scale vortices, i.e. the reversed flow towards the penstock, is crucial to prevent damaging the hydropower plant. The importance of limiting the reversed flow scales with the flow momentum in the penstock. - Literature, e.g. Ruprecht et al. [5] and Hyun et al. [2], suggests reducing the dead water region by tightening the manifold geometry, thereby not providing the large-scale vortical flow structures with the space to develop. This approach cannot be adopted in the present application. Instead, the flow must be divided equally into all branch lines to guarantee flow stability at all flow rates.

Although the presented numerical methodology performed excellently for the prediction of large-scale vortical flow structures, its application can only be recommended in cases of particular interest. More than 400,000 core hours per case were needed on the Vienna Scientific Clusters (VSC) to simulate the flow and reach statistical convergence. - The inflow fluctuations have been observed to crucially influence the motion of the large-scale vortical flow structures in the pipe multifurcation. Most reliable inflow perturbations have been generated using a boundary condition based on the fluctuation recycling method, which demands a sufficient length of highly resolved mesh to guarantee the independence of the turbulent fluctuations. This strategy comes at the cost of computational resources.

5. Conclusions

Pipe multifurcations are commonly encountered in hydropower plants to divide mass flow rates as desired. The risk of flow instability in a manifold with six branches was investigated by numerical simulations at off-design operating conditions, i.e., a reduced number of active branch lines. The Large Eddy Simulation (LES) approach was adopted on a structured mesh with 120 million cells and a wall refinement satisfying $y^+ < 1$ in the entire domain. Thereby, the evolution of the vortical flow structures could be studied, which led to the following conclusions;

- Stable flow regimes were observed operating one and all six branch lines.
  - With the operation of only one branch line, low flow velocities are established at the pipe multifurcation. The flow momentum can redistribute and enter the branch line without generating large-scale flow structures.
  - No dead water regions form when all branch lines are active. Thereby, regions with large shear layers and the generation of large-scale vortical flow structures are avoided.
- Large-scale flow instabilities manifest in the pipe multifurcation when two but not all branch lines are operated. The axially incoming flow interacts with the axially closing hemisphere and flows against the main flow direction at the outer perimeter. In the spaces where the branch lines are inactive, the reversing flow interacts with the newly arriving axial flow, forming large-scale vortices.
  - The large-scale vortical flow structures exhibit extended motion. In the interaction process with non-operational branch lines, the large-scale vortical flow structures can burst and reestablish after a short time.
  - The flow recirculation in the dead water region gives rise to flow instability, which could be suppressed by isolation with dividing inserts.

Acknowledgments

The computational results presented have been achieved in part using the Vienna Scientific Cluster (VSC). The authors acknowledge the financial support through the Österreichische Forschungsförderungsgesellschaft (FFG) under the projects 'AxFeeder' (project number 888084).

References

[1] Kougias I, Aggidis G, Avellan F, Deniz S, Lundin U, Moro A, Muntean S, Novara D, Pérez-Díaz J I, Quaranta E *et al.* 2019 *Renewable and Sustainable Energy Reviews* **113** 109257
[2] Hyun J J, Choi J W, Jang W G, Cho Y, Kim Y I, Cho T Y, Cho I J and Kim Y J 2019 *IOP Conference Series: Earth and Environmental Science* vol 240 (IOP Publishing) p 052017
[3] Staubli T and Hug S 2012 *17th Inter. Seminar on Hydropower Plants-Pumped Storage, Vienna, Austria*
[4] Decaix J, Drommi J L, Avellan F and Münch-Alligné C 2022 *IOP Conference Series: Earth and Environmental Science* vol 1079 (IOP Publishing) p 012106
[5] Ruprecht A, Helmrich T and Buntic I 2004 *Modelling Fluid Flow: The State of the Art* (Springer) pp 229–246
[6] Kirschner O, Wack J, Junginger B, Junginger J, Ruprecht A and Riedelbauch S 2019 *WasserWirtschaft* 44–47
[7] Guo X, Cheng H, Wang H, Cheng Y and Sun M 2019 *Energies* **12** 2941
[8] Morabito A, Wu C, Sigali S and Vagnoni E 2022 *ViennaHydro 2022*
[9] Aguirre C A, Camacho R G R, de Oliveira W and Avellan F 2019 *Renewable Energy* **131** 197–207
[10] Pope S B 2000 *Turbulent flows* (Cambridge University Press) ISBN 9780521598866
[11] Celik I, Cehreli Z and Yavuz I 2005 *Journal of Fluids Engineering* **127** 949–958
[12] Celik I, Klein M and Janicka J 2009 *Journal of Fluids Engineering* **131** 031102